THE PENNSYLVANIA STATE UNIVERSITY

SCHREYER HONORS COLLEGE

DEPARTMENT OF MECHNICAL AND NUCLEAR ENGINEERING

ELECTRON AND OPTICAL MICROSCOPY ANALYSIS OF MODEL ZIRCONIUM ALLOY OXIDES

JACOB LOUIS PLANINSEK

SPRING 2011

A thesis in partial fulfillment
of the requirements
for a baccalaureate degree
in Nuclear Engineering
with honors in Nuclear Engineering

Reviewed and approved* by the following:

Dr. Arthur Motta
Chair of Nuclear Engineering
Thesis Supervisor and Honors Advisor

Dr. Igor Jovanovic
Associate Professor of Nuclear Engineering
Reader

*Signatures are on file in the Schreyer Honors College.

Abstract

Zirconium alloys are among the most important materials used in light water reactors. Zirconium alloys are used for in core structures and for nuclear fuel cladding which is the first barrier retaining radioactive fission products. The corrosion properties of zirconium alloys are the primary factor determining the life and integrity of these components. The corrosion mechanisms of pure zirconium are not well known. The oxide growth kinetics quickly transition from stable growth to breakaway growth and develops instabilities in oxide growth in the form of dendrites growing into the metal. Optical microscopy performed in this study has determined that the dendrites advance through the grain boundaries. An oxygen layer that advances ahead of the oxide is observed when the sample is well into the breakaway oxide regime. The development of the oxygen layer is key to determining the transition from stable to breakaway oxide growth. Pure zirconium can contain up to 30% oxygen as interstitials in the crystal lattice. During stable oxide growth oxygen could gather in higher concentrations at the grain boundaries that cause the oxide to advance in these boundaries and destabilize the oxide growth. The uneven stress caused by the oxide advancement could be responsible for breakaway, as evidence by the cracks observed behind the oxide in the grain boundaries.

Acknowledgments

I would like to acknowledge Dr. Arthur Motta for his guidance and providing me the opportunity to perform this work, Adrien Couet and Kimberly Colas for imparting their knowledge, Maria Klimkiewicz and Trevor Clark for their help, and my family for their support through my educational career.

Table of Contents

List of Figures

List of Tables

1 Introduction and Literature Review

1.1 Introduction

The commercial nuclear industry operates pressurized water reactors (PWR) with an outlet temperature of 360˚C. The uranium dioxide fuel is housed in alloyed zirconium tubing referred to as the nuclear fuel cladding. The fuel cladding is the primary containment for the fuel and fission products. Zirconium was selected for these light-water reactor applications primarily for its low neutron absorption; however, pure zirconium has poor corrosion resistance and it must be alloyed to keep corrosion within limit in the environment of light water reactors. The development of these alloys has been a trial and error process with the development of a major advancement the result of accidental contamination of zirconium with stainless steel.

Zirconium has a very strong affinity for oxygen, which presents a significant hurdle for its use in an oxygen rich environment like a nuclear reactor. The alloying of zirconium has resulted in significant advancements in suppressing corrosion, although the corrosion mechanisms are not well understood. The process of oxidation is primarily understood and depicted in Figure 1-1. The process starts at the water metal interface where dissolved oxygen is absorbed into the oxide surface due to vacancies created by oxide diffusion toward the metal.

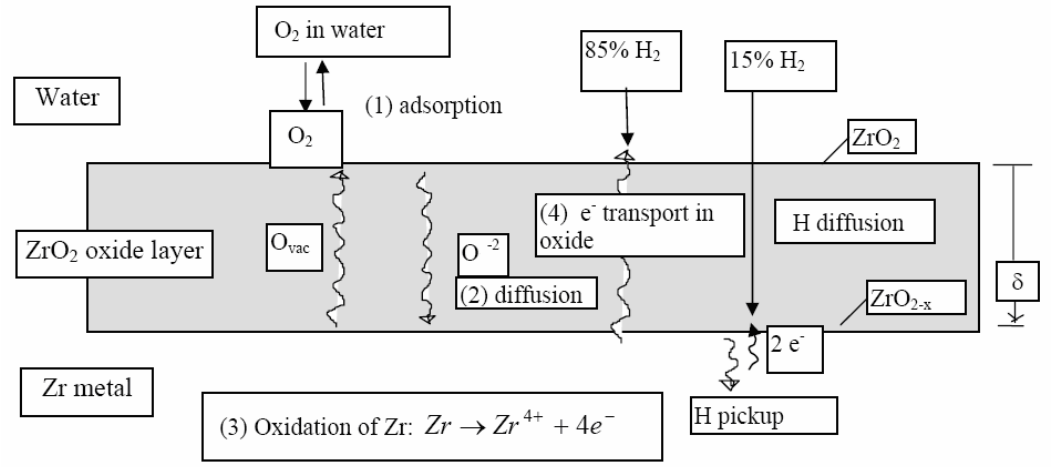

Figure 1-1 Schematic of reactions taking place during uniform corrosion of zirconium[1].

The oxygen reacts with the metal in which electrons are freed, diffuse to the oxide surface and react with water to create more oxygen ions and release hydrogen gas. Zirconium has a Pilling-Bedworth ratio of 1.56, which means that the consumption of 1μm of zirconium due to oxidation results in the formation of 1.56 μm of zirconium oxide. Although most of the volume expansion occurs in the vertical direction, this large oxide growth ratio creates stresses in the oxide and results in cracks and potential loss of protectiveness. The stability of the oxide can be determined from the structure of the oxide relative to the cracks caused by the stresses endured by the oxide. Studying the oxide structures and oxide metal interface of model zirconium alloys can establish relationships between oxide behavior and oxide structures. Figure 1-2 shows the regimes of oxide growth in unalloyed zirconium.

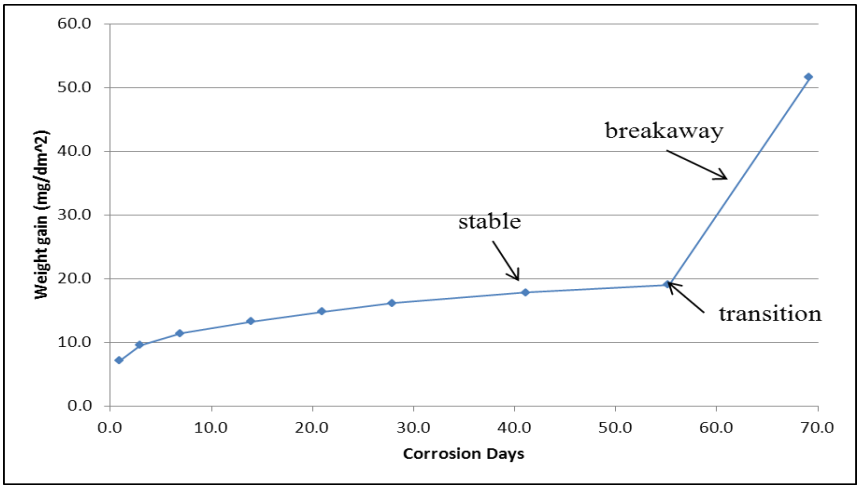

Figure 1-2 Diagram showing the three regimes of oxide growth in unalloyed zirconium.

The stable oxide regime has been found to form a uniform oxide layer at the metal surface. The transition from stable to breakaway is caused by mechanical stress building up during the stable oxide growth and cracks then develop in the oxide to relieve this stress. The cracks in the oxide are not uniform and allows irregular oxide advancement. The non-uniform oxide growth causes uneven stresses that in turn cause the oxide to break away [2]. The study conducted here analyzes the phenomena of oxide transition.

1.2 Previous studies on zirconium alloy corrosion properties

The individual role each alloying element plays in oxidation is not yet understood relative to corrosion rate. Studies have been performed where alloying element and concentration have been varied to determine their ability to suppress corrosion [3]. The alloying element and concentrations make critical differences in the corrosion properties of zirconium. Model zirconium alloys have been studied using many techniques including synchrotron radiation which analyzes the microstructure of the alloy and oxide [4]. This study related alloying elements with material phases and corrosion resistance.

The use of Orientation Imaging Microscopy (OIM) is well known for analyzing non-composite zirconium samples. Studies have been performed to show the effects of deformation on the grains of zirconium with OIM [5] . The textured zirconium samples were loaded parallel and perpendicular to the

basal plains and the true stress versus strain curved were compared. OIM was used to confirm the texture orientation. Others have studied the grain boundary development of zirconium during grain growth [6]. OIM was used to compare the grain characteristics of zirconium annealed with varying parameters. The methods used to preparing zirconium for OIM are similar in several papers and are crucial for this study.

1.3 Motivation

Much of the previous studies performed on zirconium oxidation mechanisms study the oxide and metal phases or relate alloys to corrosion rates. Zirconium oxidation mechanisms are not entirely understood. The phenomenon of transition from stable to breakaway is most dramatically seen in pure zirconium. To understand this phenomenon could have far reaching implications for better understanding the transition in alloyed zirconium and ultimately leading to design alloys with better corrosion properties.

The goal of this work is to gain information about zirconium undergoing transition from stable to breakaway oxide growth. In this experiment autoclave corroded model zirconium alloys will be prepared for observation with electron and optical microscopy. The samples will be cross sectioned, mounted, and polished to provide a surface that can be analyzed. The surface requirements vary with the techniques used to analyze the samples. Of the techniques used in this study, OIM requires the highest quality of surface preparation. OIM requires a flat and damage free surface. The composite nature of these samples presents difficulties for sample preparation. The hard oxide and soft metal provide the greatest hurdle for OIM sample preparation. The oxide metal interface is the area of interest to determine the stability of the oxide and this area will present the greatest challenge during sample preparation due to the significantly different polishing characteristics of the oxide and metal.

The electron microscopy will be employed to analyze high magnification oxide and oxide metal interface characteristics. Polarized light microscopy will allow the characterization of the zirconium metal grains although it will only yield information as to grain boundary location. OIM has the capability to

map the grain orientation of the zirconium metal. The dendrites observed advancing into the metal ahead of the oxide layer will be characterized relative to grain boundaries and grain orientation using these techniques. The degree of oxide advancement may be related to the grain disorientation.

2 Methodology

2.1 Sample fabrication

The corrosion coupon samples were prepared in a previous study in which model zirconium alloys were constructed through a meticulous process to control elemental composition, grain size, texture, and material phase [3]. The model alloys were fabricated into 25x20x0.6 mm coupons shown in Figure 2-1.

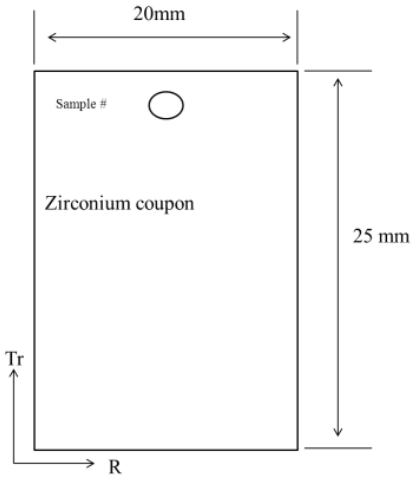

Figure 2-1 Fabricated zirconium alloy corrosion coupon dimensions.

The samples were fully recrystallized after fabrication producing a grain size of 10-15 μm, and then corroded in controlled autoclave environments. The autoclave created temperature and pressure conditions relevant to the performance seen in commercial nuclear reactors. The autoclave exposed the zirconium coupons to 360ºC water at 18.7 MPa. The samples were carefully monitored during autoclave corrosion to track weight gain over time.

2.2 Analysis Techniques

The samples were cross-sectioned and polished as detailed in Appendix A for analysis with electron and optical microscopy. The electron microscopy was performed at the Penn State materials

characterization lab with a Hitachi S-3500 Scanning Electron Microscope (SEM) equipped with OIM instrumentation. The optical microcopy was performed with a Zeiss Axiovert 200 Mat microscope equipped with polarizing features.

2.2.1 Electron Microscopy

The SEM is a powerful tool used to analyze the oxide and oxide metal interface. In particular the use of secondary electrons provides an image which can yield information about the surface topography and structure. The backscattered electron images yield information about the elemental makeup of the sample providing contrast between low and high atomic mass elements. The Hitachi S-3500N SEM used in this project is shown in Figure 2-2.

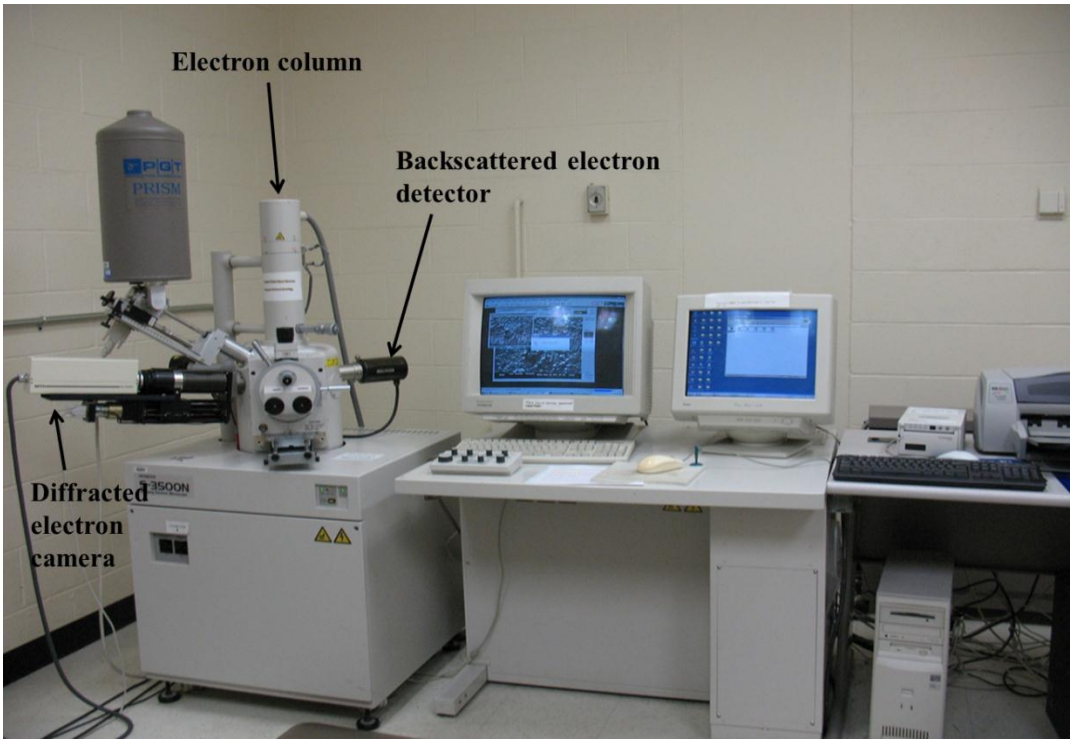

Figure 2-2 Hitachi S-3500N SEM used for imaging and OIM.

For this project, backscattered electrons images are used to gain information about the oxide metal interface and oxide structure. This SEM is also equipped with OIM instruments which can create grain orientation maps of the sample surface. The OIM is based on Electron Backscatter Diffraction

(EBSD). EBSD follows Bragg's law as the electrons diffract from the crystalline structure. The sample is set up at a 70˚ angle relative to the electron beam, as shown in Figure 2-3 where the electrons diffract through the sample and onto a phosphorous screen.

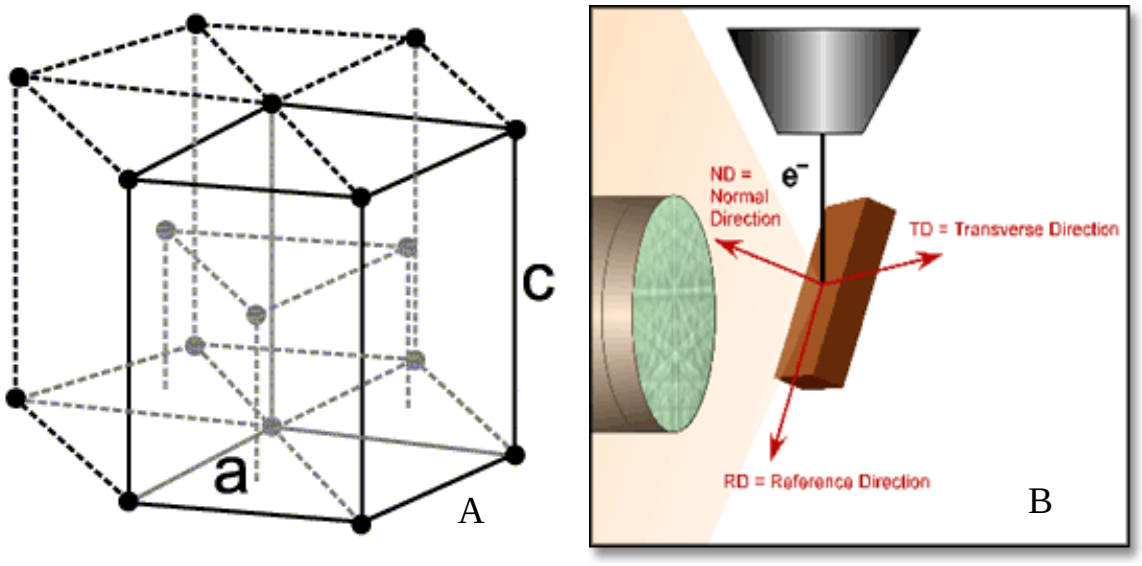

Figure 2-3 (A) Zirconium hcp unit cell with a=3.2313Å and c=5.1479Å [7], (B) Sample setup inside SEM to perform OIM.

The detected pattern is indexed by the OIM software to determine the orientation of the crystal which diffracted the beam. The beam is moved in a grid pattern over the sample creating a map of the grain orientations throughout the sample surface.

2.2.2 Optical Microscopy

The optical microscope is a particularly powerful instrument for zirconium. The anisotropic hexagonal close packed (hcp) crystalline structure of zirconium allows the grains to be revealed with polarized light. The polarized light interaction with the hcp crystalline structure causes contrast (light wavelength shifts) between grains of varying orientation. This technique is particularly important for this study.

3 Metallography

3.1 Sample preparation

The initial sample dimensions were 25 by 20 by 0.6 mm. The samples were sectioned using a low speed diamond saw, as shown in Figure 3-1 to produce samples for electron and optical microscopy analysis.

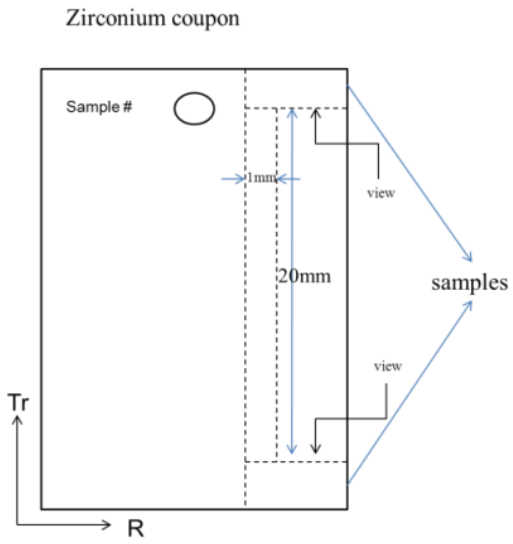

Figure 3-1 Zirconium coupon sectioned for samples.

The samples were clipped together and mounted in 1.25 inch diameter epoxy. The samples were clipped together to promote oxide integrity during the polishing sequences and a 1.25 inch diameter epoxy mold was used so the samples could be polished in an Allied triple polisher. The samples underwent various high degrees of polishing, as required by the analysis techniques. Of the three techniques used for this study the SEM required the lowest degree of polishing, which necessitated maintaining the oxide layer and undamaged oxide metal interface. For some of the thin oxide samples nickel plating was implemented to ensure oxide integrity, although through guidance from polishing authorities such as Leco, Buehler, and Allied a polishing sequence was developed that made nickel plating unnecessary. The sample preparation for polarized light microscopy requires a much higher degree of polishing than that

required for SEM. Polarized light must interact with the crystalline structure to yield results and therefore nearly all surface damage from sample preparation must be removed. This process involves carefully monitoring each polishing sequence to ensure that each step to finer polishing fully removes the damage from the previous step. The final step in polishing is 0.05μm colloidal silica. This step requires extended amount of time to remove the damage from previous step due to its slow material removal rate for zirconium.

The sample mounting for OIM is very different than that for polarized light or SEM. The surface requirements for this technique are of the highest standard. The extremely small interaction volumes of the electron for this technique require the surface to be completely free of damage.

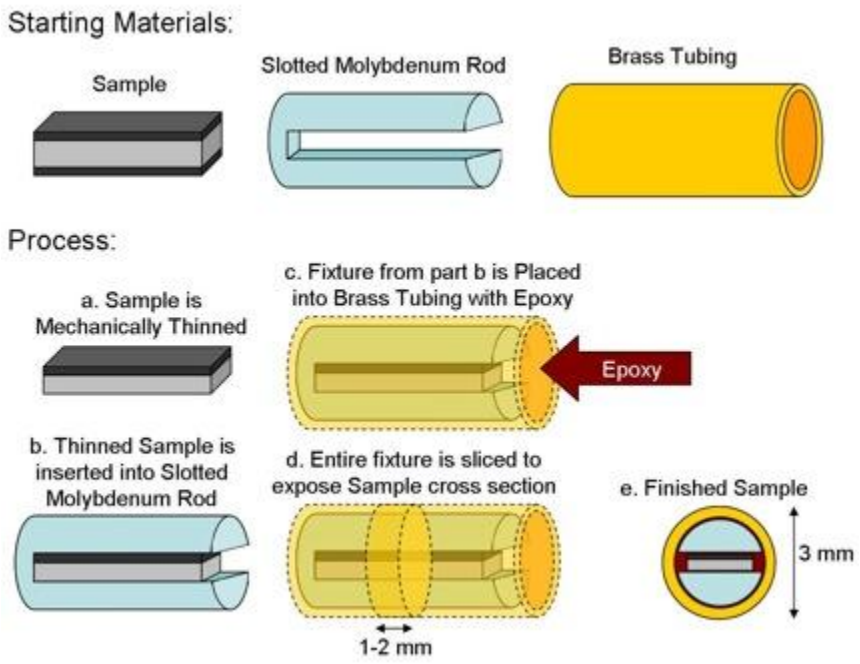

Figure 3-2 Sample preparation technique used for OIM specimens.

The samples are prepared inside a 3 mm brass tube with a molybdenum rod holder, as shown in Figure 3-2. This sample setup is required for the sample to be correctly aligned and able to be mounted in the ion mill. Although the polishing technique is similar to that use for polarized light microscopy in the details of removing damage, molybdenum is harder than zirconium so attention must be paid to maintain

surface flatness. Once the sample surface is as damage-free as mechanical polishing will allow, the sample must be ion etched using a Fischione Ion Mill (Figure 3-3) to remove the remaining damage without compromising the surface flatness. Only when the sample is flat and without damage can OIM be successfully completed.

Figure 3-3 Fischione Low Angle Ion Mill model 1010 used to prepare samples for OIM.

Because the samples are a composite material containing both very hard zirconia and relatively soft zirconium, this is an extremely difficult process, especially because the area of interest is the oxide metal interface. The process of non-composite zirconium OIM has been previously accomplished by other researchers using several different techniques. The published methods include lightly etching the sample surface with hydrofluoric and nitric acids to remove the damage from mechanical polishing [8], final polishing with an attack solution composed of colloidal silica mixed various chemicals or acids [5], special vibratory final polishing [9], and mechanical polishing then electropolishing in perchloric and acetic acid [6]. These published methods could not be applied to the samples in this study due to the presence of the oxide layer. The process of etching or electropolishing would leave a step between the oxide and metal, which prevents the study of the relation between the metal grains and oxide. The process of attack polishing was not possible to conduct in the facilities available due to health risks associated with the chemicals; also, attack polishing could have created an irregular surface due to uneven attack rates. The vibratory polisher specified was not an option due to the extreme cost. The process for

chemically removing the sample's oxide was investigated, only to find that any chemical capable of attacking zirconia has a higher attack rate for zirconium [10] thus resulting in the removal of the metal before the oxide. The only other OIM sample preparation techniques besides what is shown here in this case is using the Focused Ion Beam (FIB) to section a sample. The other major issue in dealing with zirconium and OIM is that the sample oxidizes and the sample surface degrades with time leaving a window of only a few hours after sample prep to perform OIM. The detailed polishing sequences are included in Appendix A.

3.2 Chemical Etching

Samples with dendrites were initially etched to expose grains, and investigate whether the dendrites follow grain boundaries. The samples were initially polished following the SEM sample preparation techniques before being etched to ensure oxides were intact. The samples were swab-etched for 10 seconds with 45% H_2O, 45% Nitric acid (70%), 10% Hydrofluoric acid (52%) [11]. This etching procedure proved to be too aggressive. The zirconium was well below the oxide surface and under the microscope the oxide could not be related to the grain boundaries. A new etching solution was prepared after referring to the corrosion handbook [12]. The new solution was composed of 40 mL Nitric acid (70%), 60 mL H_2O, and 3 drops (~0.1 mL, ~400 ppm) Hydrofluoric acid (52%). This solution was used to swab etch samples for approximately 10-15 seconds. Although this process still left a step between the metal and oxide, the step was small enough that it did not impede the relation between the oxide and metal to be studied with polarized light microscopy. Several other solutions were prepared including substituting hydrogen peroxide for water and varying the hydrofluoric acid concentration that created large steps between oxide and metal [13]. It should be noted that the solution used above to etch samples could only be used for crystal bar zirconium due to uneven etching with other alloys, including sponge zirconium which has a minor iron impurity. This solution was further altered for the application of OIM. The large angle of electron beam incidence proved the above etching left too large of a step. The etching solution used to etch crystal bar zirconium for OIM was 20 mL Nitric acid (70%), 80 mL H_2O, and 1

drops (~0.1 mL, ~150 ppm) Hydrofluoric acid (52%). The sample was swab etched for 20 seconds in this solution and produced a step between the oxide and metal on the order of a few microns which was suitable for OIM although it was still not achieved at the oxide metal interface.

4 Analysis of Imaging

The quality of information gained from these various techniques depends greatly on the degree the samples are polished. Generally better polishing yields higher quality information. Many samples of various alloys were analyzed with the SEM. The samples listed in Table 4-1, Table 4-2, and Table 4-3 are ones that pertain to this study.

Table 4-1 Alloy 42 crystal bar zirconium corrosion days and weight gain.

Samples	composition	Corrosion days	Weight gain (mg/dm^2)
42-12	Crystal bar Zr	7	10.5
42-15		3	36
42-10		69.25	91.24
42-13		32	658.7

These samples were taken at different steps corrosion process. The samples in this case with less than approximately 20 mg/dm^2 are in the stable regime and the samples above this weight gain have transitioned to the breakaway regime.

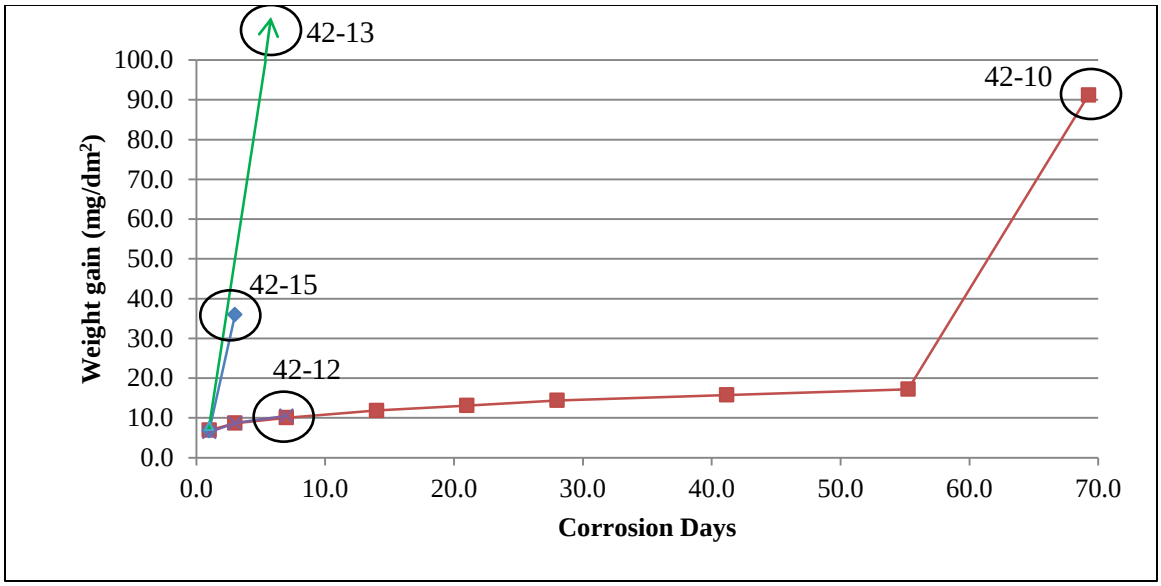

Figure 4-1 Alloy 42 Crystal bar zirconium weight gain versus corrosion time.

The samples 42-10, 42-15, and 42-13 are post transition and 42-12 is pre-transition, as shown in Figure 4-1 . The transition point can clearly be seen in sample 42-10 where the weight gain slope dramatically changes. The sample 42-13 end point is not shown in this figure due to its extreme weight gain.

Table 4-2 Alloy 41 sponge zirconium corrosion days and weight gain

Samples	Alloy	Corrosion days	Weight gain (mg/dm²)
41-9	Sponge Zr	69	51.6
41-11		14	68.9
41-12		7	15.1
41-15		3	27.3

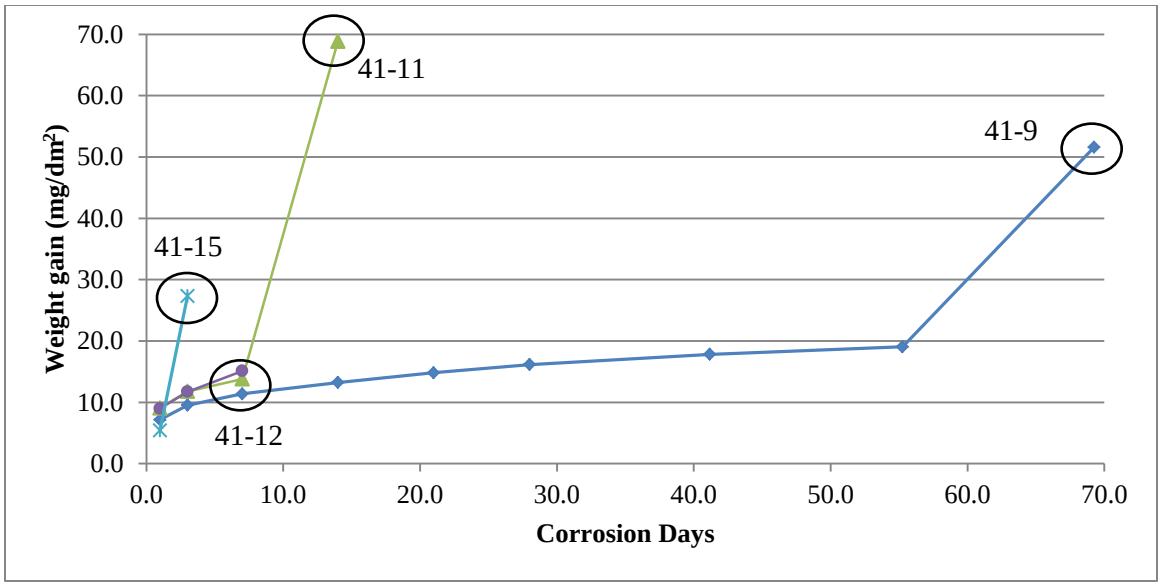

Figure 4-2 Alloy 41 sponge zirconium weight gains versus corrosion time.

The corrosion properties of sponge zirconium (alloy 41) closely resemble those of crystal bar zirconium (alloy 42) as shown Figure 4-1and Figure 4-2. The sponge zirconium has an iron impurity content of approximately 300 ppm whereas that of crystal bar zirconium has 50 to 100 ppm. Zircaloy-4 has an alloying content of 1.5% Tin, 0,1% Chromium, and 0.2% Iron and the samples chosen to be analyzed are shown in Table 4-3. These samples cover the range of weight gain from the start of the corrosion cycle to the end.

Table 4-3 Alloy 43 Zircaloy-4 corrosion days and weight gain.

Samples	composition	Corrosion days	Weight gain (mg/dm²)
43-3	Zircoloy-4	240	68.1
43-8		28	20.5
43-11		55	26.2
43-16		371	100.6

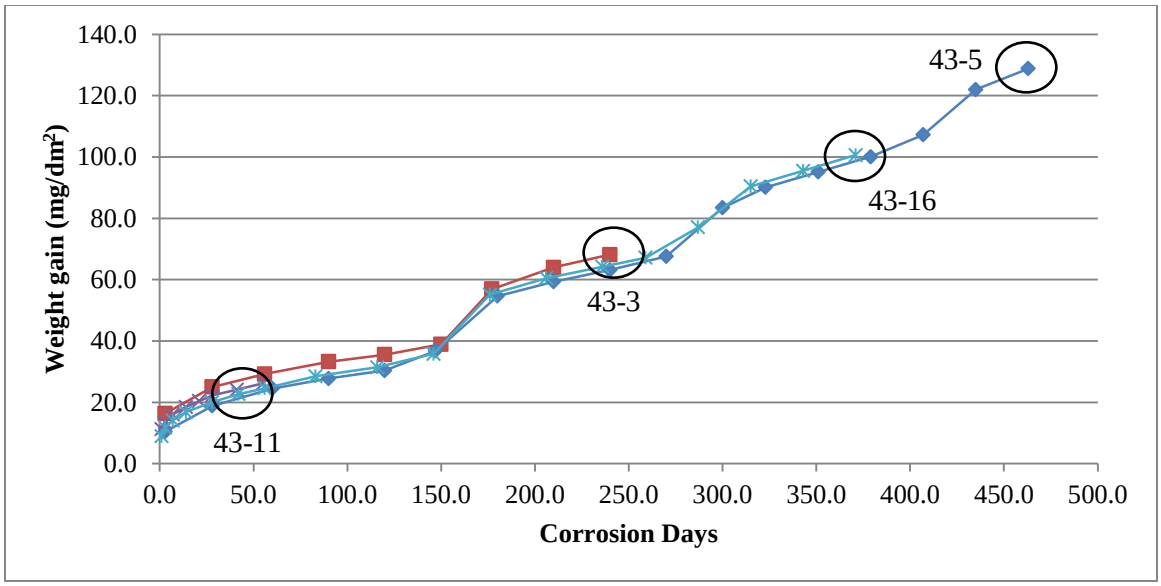

Figure 4-3 Alloy 43 Zircaloy-4 weight gains versus corrosion time.

Figure 4-3 shows the weight gain versus time for the zicaloy-4 samples. Zircaloy-4 experiences the unique trend of undergoing transition to breakaway although it recovers back to stable upon the transition.

4.1 Scanning Electron Microscopy Analysis

The SEM yields information based on the sample's chemical composition and surface topography. This technique yields important information about the oxide structure and metal oxide interface. The large Pilling-Bedworth ratio of 1.56 causes stresses in the oxide which lead to crack development. The cracks in these oxides can determine the stability of the oxide.

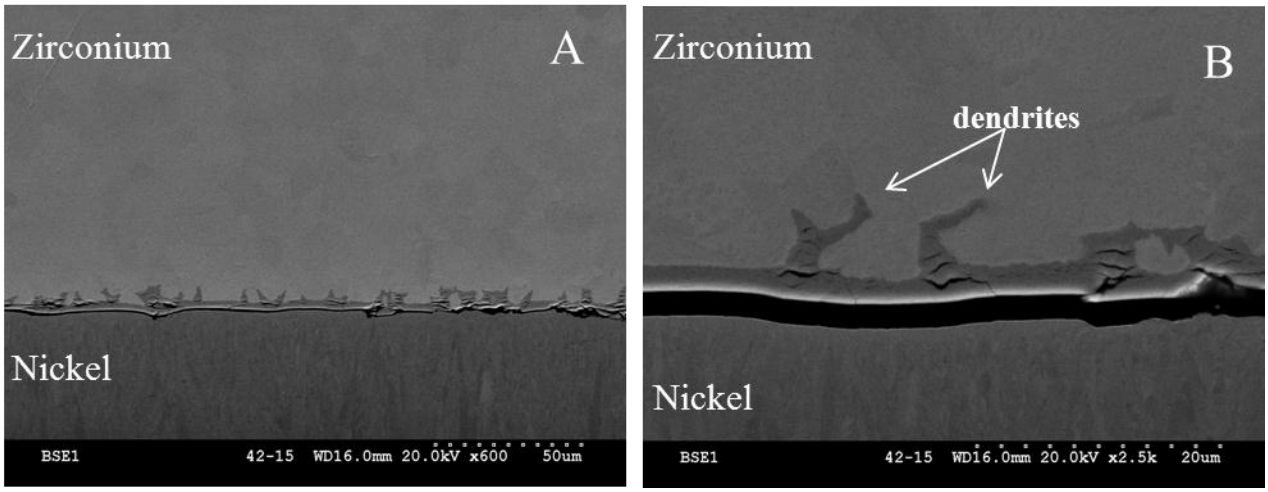

Figure 4-4 SEM images of crystal bar zirconium corroded in 360ºC water for 3 days with 36 g/dm^2 weight gain (sample 42-15) shows unstable oxide advancement, with dendrites at A) 600x magnification and B) 2500x magnification.

Figure 4-4 shows the crystal bar zirconium sample corroded for 3 days in 360ºC water. Oxide dendrites (arrowed in the picture) have formed at the oxide-metal interface, indicating preferential propagation of the oxide ahead of the main oxide front. These dendrites are associated with transition to faster corrosion kinetics associated with breakaway. Also the dendrites are speculated to propagate at the grain boundaries. The grains can faintly be seen in these images although not clearly enough to draw any conclusions on the relationship of dendrites to grain boundaries. The cracks seen behind the oxide dendrites show the start of breakaway oxide kinetics. The oxide behind the dendrites will separate causing loss of protective oxide and increase oxide kinetics.

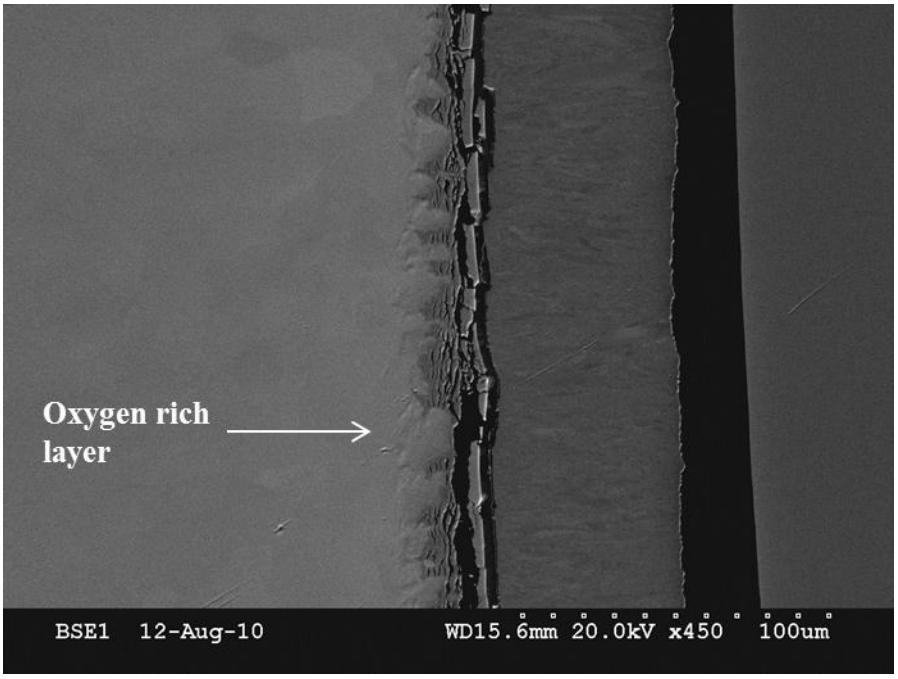

Figure 4-5 SEM image of crystal bar zirconium corroded in 360ºC water for 69 days with 91.2 mg/dm^2 weight gain shows the initial development of the oxygen layer advancing ahead of the oxide in sample 42-10.

Figure 4-5 shows crystal bar zirconium corroded in 360ºC for 69 days with 91.2 mg/dm^2 weight gain and the initial observable oxygen rich layer formed ahead of the oxide front. The large lateral cracks and separation between oxide cracks clearly displays breakaway characteristics as the external oxide no longer provides protection from water ingress. The oxygen rich layer ahead of the oxide front is believed to be a solid solution of oxygen interstitials in the zirconium matrix. Zirconium can contain up to 30% oxygen as interstitials in solid solution [2].

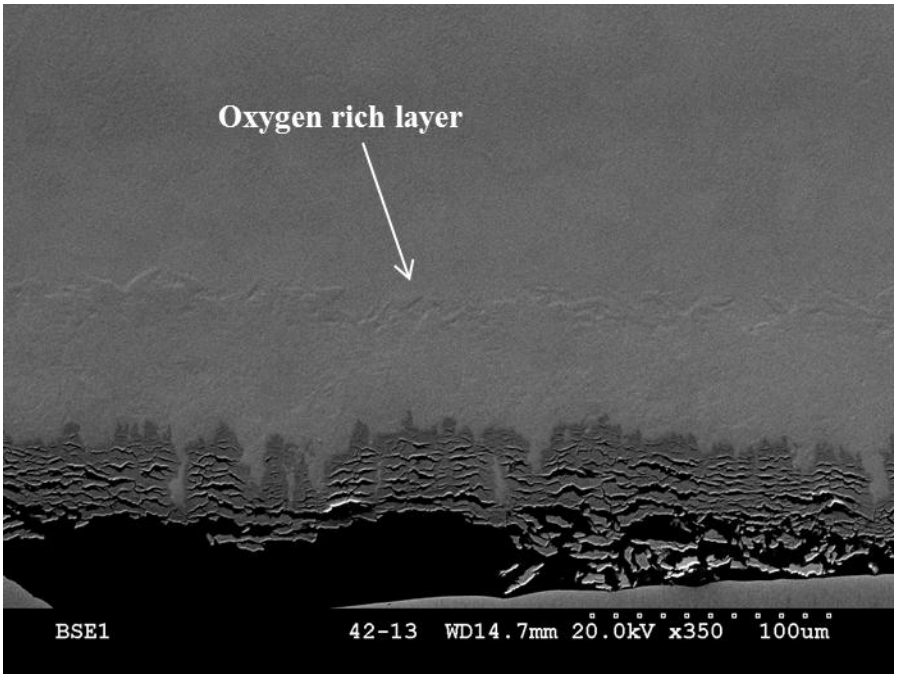

Figure 4-6 SEM image of crystal bar zirconium corroded in 360ºC water for 32 days with 653.5 g/dm^2 weight gain showing large oxygen layer ahead of oxide in sample 41-13.

Figure 4-6 shows crystal bar zirconium corroded in 360º water for 32 days and the large oxygen rich layer that has developed ahead of the oxide front. The numerous large lateral cracking in the oxide shows the oxide flaking off. This sample is very far into the breakaway regime. The oxide layer composed of ZrO_{2-x} would support the kinetics of zirconium oxidation. The diffusion of oxygen into zirconium creates ZrO_{2-x} which can readily transform into ZrO_2 at the oxide metal interface. During breakaway oxidation the zirconium is oxidized at a very rapid rate which would relate to the oxygen layer making this rate of ZrO_2 production possible. The protective nature of alloyed zirconium prevents it from experiencing this oxygen layer.

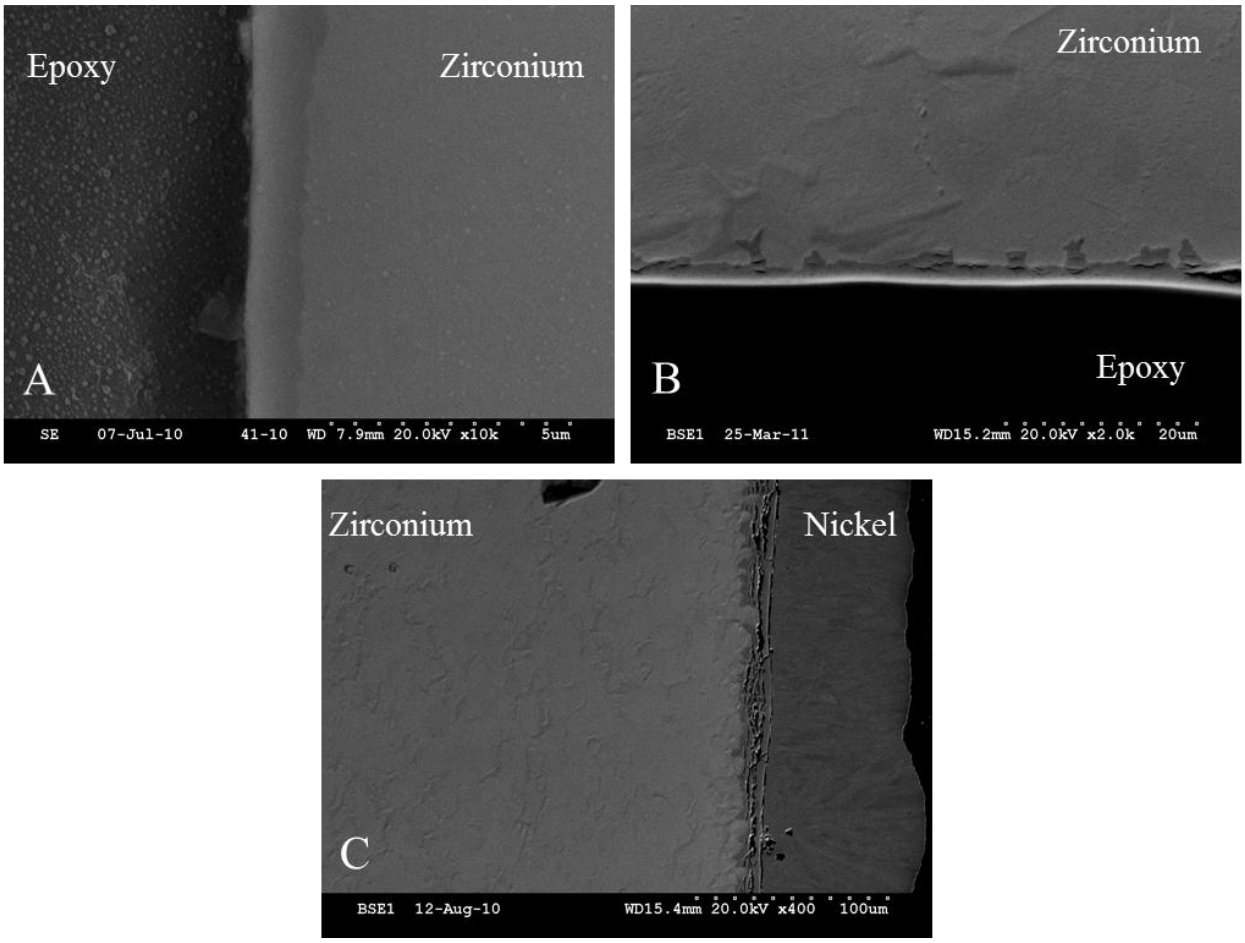

Figure 4-7 SEM images of Alloy 41 sponge zirconium corroded in 360ºC water. A) 14 corrosion days and 16.3 mg/dm^2 weight gain sample 41-10, B) 3 corrosion days and 27.3 mg/dm^2 weight gain sample 41-15, and C) 69 corrosion days and 51.59 mg/dm^2 weight gain sample 41-9.

Similar observations can be made in sponge zirconium. Figure 4-7 shows several sponge zirconium samples corroded in 360ºC. Figure 4-7 A shows the protective uniform oxide that results from the stable oxide growth, B displays the oxide advancement as dendrites form just after transition to breakaway, and C shows the oxide well after the oxide transition. In this case the oxide no longer advances as dendrites and the remaining oxide catches up with the dendrites. The same dendrite formation as in alloy 42 is observed although the oxygen layer is not as readily seen. The higher iron impurity may have a role in preventing the uniform oxide layer development; although samples examined for sponge

zirconium do not exhibit the extreme corrosion as crystal bar zirconium and therefore a large oxygen layer may not have been observed in sponge zirconium.

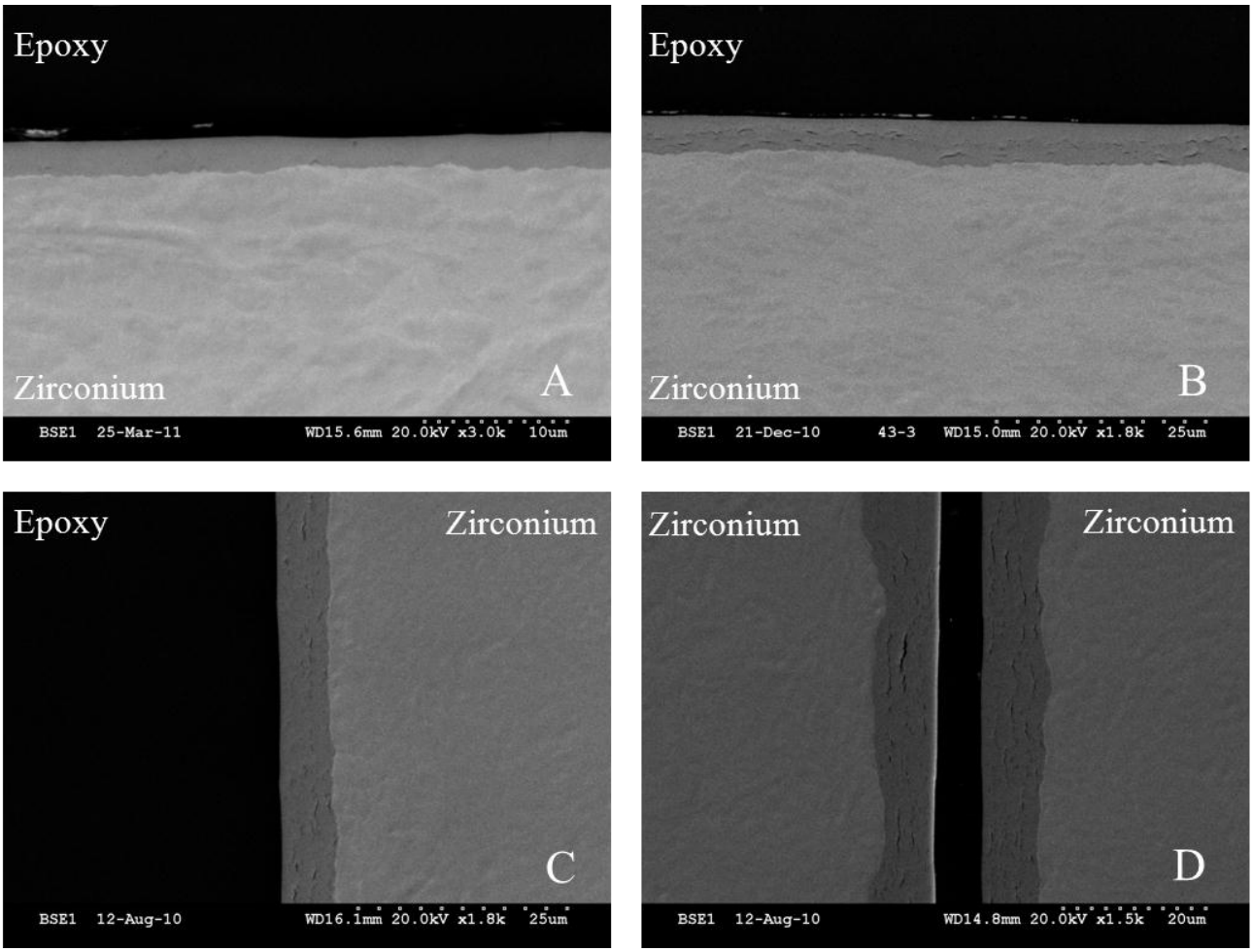

Figure 4-8 SEM images of Alloy 43 Zircaloy-4 corroded in 360ºC water. A) 28 corrosion days and 20.5 mg/dm^2 weight gain sample 43-8, B) 55 corrosion days and 26.8 mg/dm^2 weight gain sample 43-11, C) 240 corrosion days and 68.1 mg/dm^2 weight gain sample 43-3, and D) 371 corrosion days and 100.6 mg/dm^2 weight gain sample 43-16.

Figure 4-8 shows the oxide progression over time for Zircaloy-4 samples. Image A shows the oxide layer before the first transition and the oxide is a thin uniform layer. Image B shows the oxide just after the first transition where cracks from the transitions can be observed. Image C displays the oxide after the second transition and similar to image B the cracks from transitions can be seen. Image D shows the oxide after the third transition and the cracks from each transition are seen. The uniform corrosion of Zircaloy-4 displays the alloys ability to recover to a stable oxide regime after the transition point.

The samples can be etched to show the three dimensional structure of the oxide. The following samples were etched with two different solutions and this reflects in the size of the step between oxide and metal.

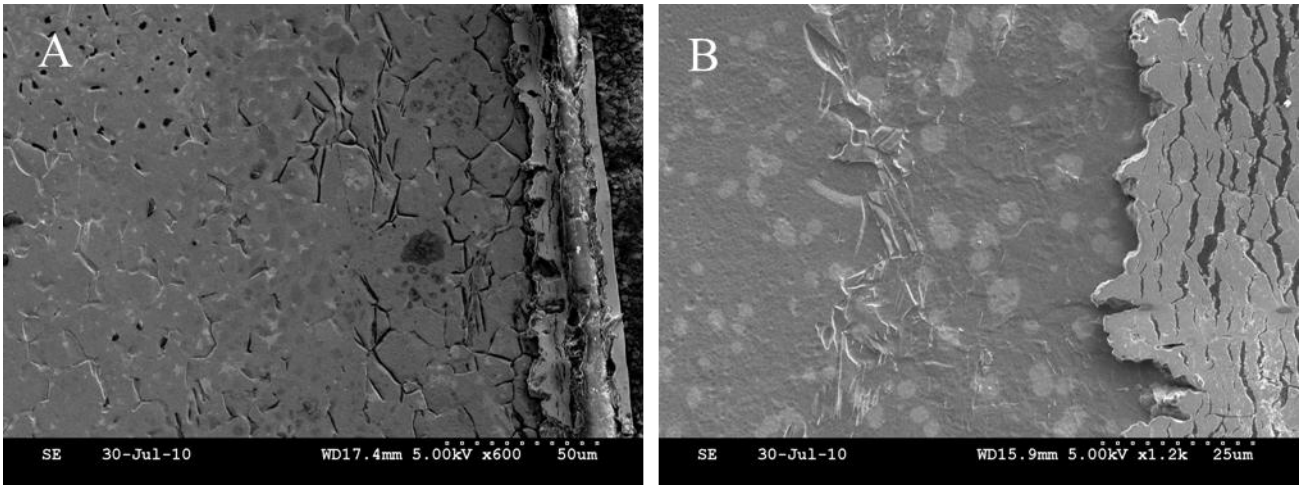

Figure 4-9 SEM images of chemically etched sponge zirconium and crystal bar zirconium samples corroded in 360°C water, A) sample 41-9, 51.59 mg/dm^2 weight gain etched in solution A and B) sample 42-13, 658.73 mg/dm^2 weight gain etched in solution B.

Figure 4-9 shows the samples after chemical etching. Image A is sponge zirconium well past transition and the valleys seen in the metal are where zirconium hydrides were etched out. Image B shows a significantly smaller step between the oxide and metal due to the lower acid concentration. Solution A was 45% H_2O, 45% Nitric acid (70%), 10% Hydrofluoric acid (52%) and swab etched for 10 seconds [11] and solution B was 40 mL Nitric acid (70%), 60 mL H_2O, and 3 drops (~0.1 mL, ~400 ppm) Hydrofluoric acid (52%) and swab etched for 25 seconds.

4.2 Polarized Light Microscopy Analysis

Polarized light yields information (in the case of zirconium) by interacting with the anisotropic hcp crystalline structure and contrasting between grains of varying orientation. The information retrieved by

this technique can be used to characterize the grain size and grain boundaries in the material but not the grain orientation.

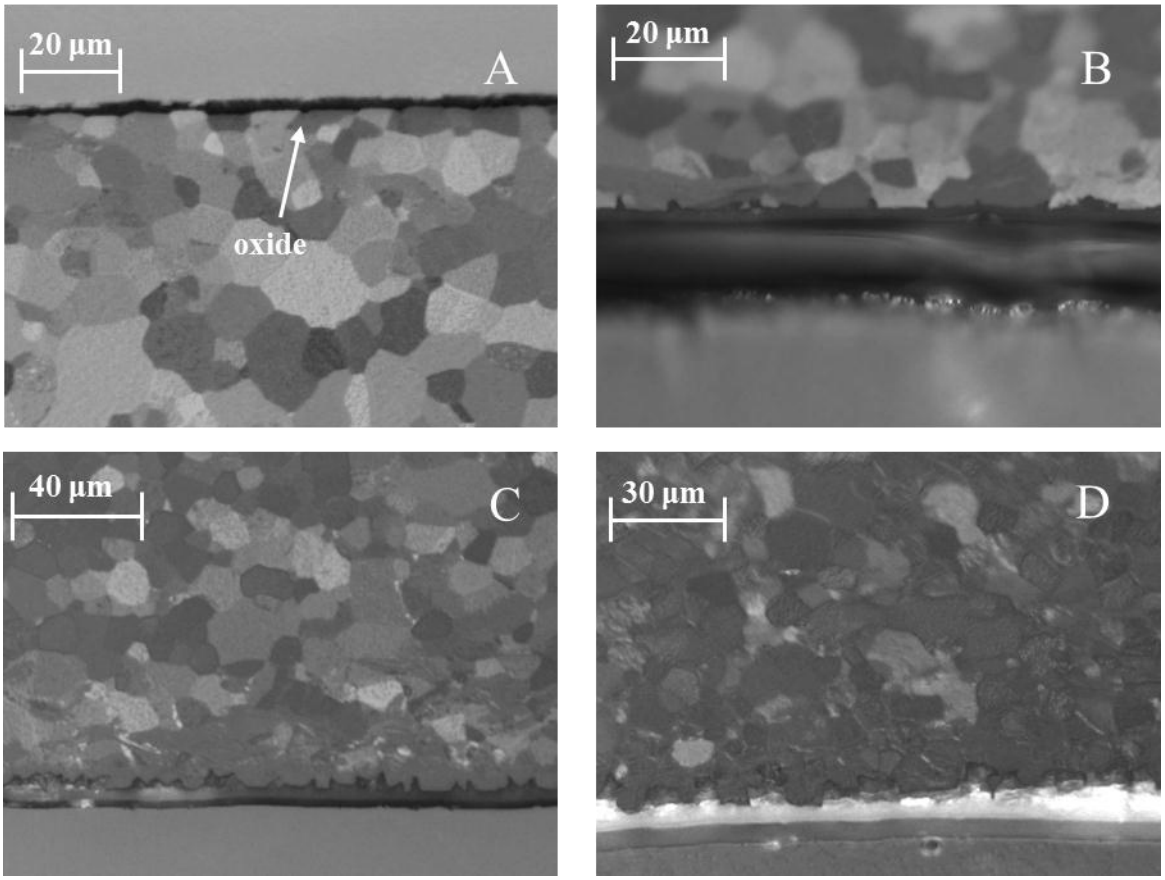

Figure 4-10 Polarized light images of Alloy 41 sponge zirconium corroded in 360ºC water. A) 7 corrosion days and 15.1 mg/dm^2 weight gain sample 41-12, A) 14 corrosion days and 16.3 mg/dm^2 weight gain sample 41-10, B) 3 corrosion days and 27.3 mg/dm^2 weight gain sample 41-15, and C) 69 corrosion days and 51.59 mg/dm^2 weight gain sample 41-9.

Figure 4-10 shows the sponge zirconium corroded in 360ºC water samples under polarized light. Image A shows the uniform thin oxide just starting to become non-uniform and entering the grain boundaries as pointed to by the arrow. Image B displays the dendrites advancing along the grain boundaries. Images C and D show oxide well into transition in which the grain characteristics change just ahead of the oxide. This change in grain characteristics is due to the oxygen ingress forming the oxygen layer. This alloy does not show the uniform oxygen layer as seen in crystal bar zirconium which could be due to the higher iron impurity or that a sample of extreme weight gain was not examined for this alloy.

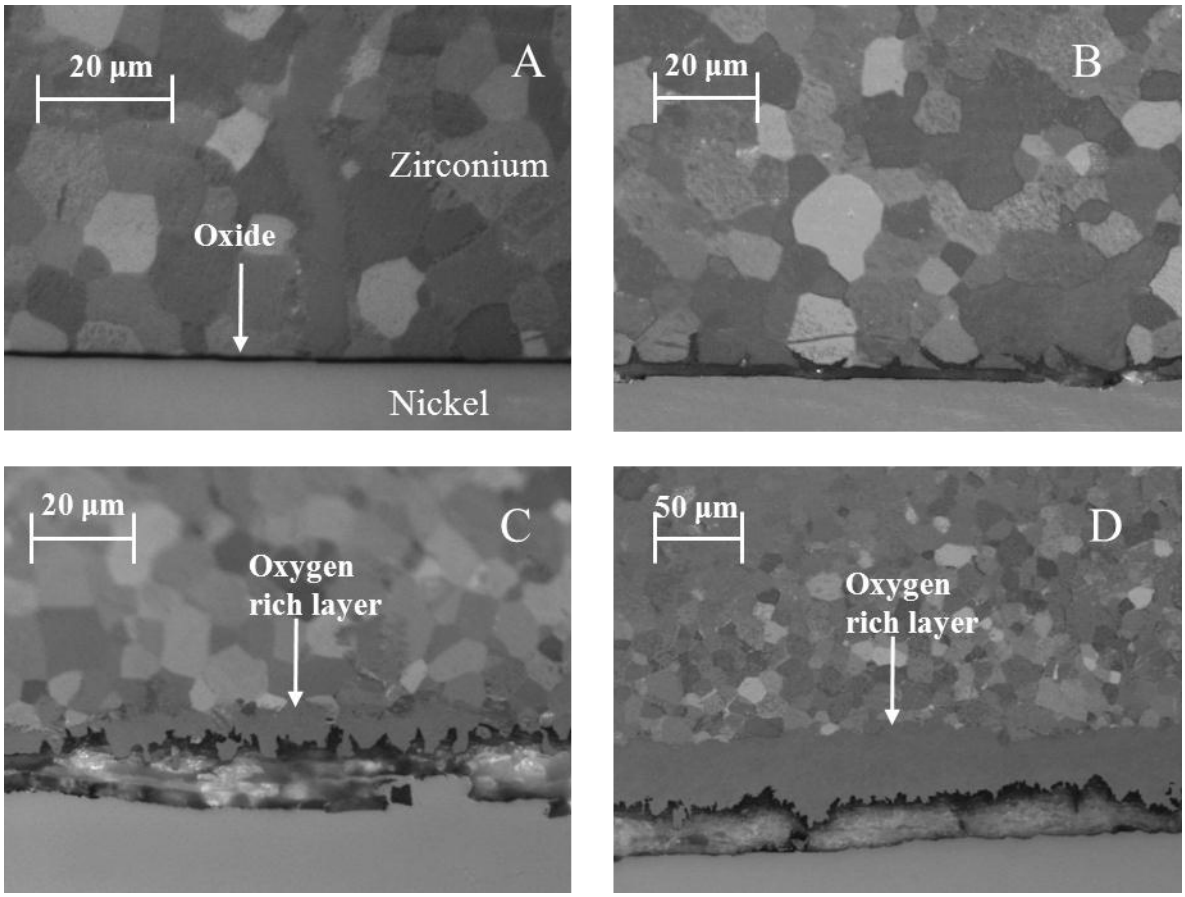

Figure 4-11 Polarized light images of Alloy 42 crystal bar zirconium corroded in 360ºC. A) 7 corrosion days and 10.5 mg/dm^2 weight gain sample 42-12, B) 3 corrosion days and 36.0 mg/dm^2 weight gain sample 42-15, C) 69 corrosion days and 91.24 mg/dm^2 weight gain sample 42-10, and D) 32 corrosion days and 658.73 mg/dm^2 weight gain sample 42-13.

Figure 4-11 shows crystal bar zirconium corroded in 360ºC water. Image A displays the uniform thin oxide layer of the stable regime as pointed to by the arrow. Image B confirms that the oxide dendrites advance through the grain boundaries as the oxide transitions from stable to breakaway. Image C shows the development of the oxygen layer ahead of the oxide front well after the oxide transition as pointed to by the arrow. Image D shows the large oxygen layer ahead of the oxide front for the sample with extreme oxidation, and the oxide front advances non-uniformly but no longer follows gain boundaries.

5 Conclusions and Future Work

5.1 Conclusions

This work studies the oxide layer formed on sponge and crystal bar zirconium oxidation mechanisms. During autoclave testing in environments relevant to the harsh reactor conditions the zirconium underwent corrosion. Samples at different stages of corrosion were studied, with special attention to the oxide-metal interface. Several conclusions can be drawn from the results of this study.

1. Optical microscopy determined that the oxide propagates through the grain boundaries at the transition point. The oxide becomes unstable once it begins to advance into the grain boundaries.
2. The oxygen layer that develops ahead of the oxide grows over time as the samples are corroded after the transition point. This oxygen layer can consist of 30% oxygen as interstitials in the zirconium matrix.
3. The advancement of the oxide into the grain boundaries could be a result of the grain boundaries having higher oxygen content due to the oxygen interstitials having preferential placement at grain boundaries. During the stable oxide growth oxygen accumulates at the grain boundaries and as the oxide begins to form in the grain boundary the transition to breakaway occurs. Cracks form behind the oxide dendrites due to stress from the uneven oxide growth and this causes the oxide to break away.
4. It has been determined that composite zirconium and zirconia samples are cannot be prepared for OIM by conventional means. The area of interest on the sample is that at the oxide metal interface where polishing methods were least successful.

5.2 Future Work

Further studies could be made using a FIB to create samples that can be examined at the oxide metal interface by OIM to determine the grain orientation relation to dendrite advancement. A FIB equipped with OIM instrumentation could create a three dimensional grain orientation map and dendrite relationship. The single cross section analyzed here may not be an accurate representation of the grain boundary oxide advancement.

The data gained from these corrosion studies could be used to design an experiment in which the transition point could be studied. The test conditions and approximate time to transition is known for many model alloys and therefore could be used to corrode samples to the transition point and study the samples at the pre and post transition points. This study could develop an understanding of transition and alloying elements effect on transition.

References

1. **Olander, Donald and Motta, Arthur.** *Light Water Reactor Materials.* 2006.

2. **Douglass, D. L.** *The Metallurgy of Zirconium.* Austria : International Atomic Energy Agency, 1971.

3. **Marcelo Jose Gomes da.** Influence of Oxide Microstructure on Corrosion Behavior of Zirconium-Based Alloys. *Ph D Thesis in Nuclear Engineering.* : Penn State University, July 2007.

4. *Microstructural Characterization of Oxides Formed on Model Zr Alloys Using Synchrotron Radiation.* **Motta, Arthur, et al.**: Journal of ASTM International, 2008, Vol. 5. JAI101257.

5. *Effects of Deformation Twinning on Energy Dissipation in High Rate Deformed Zirconium.* **Padilla, H. A., et al.** : Mettallurgical and Materials Transactions, 2007, Vol. 38A.

6. *Grain Boundary Charater Evolution During Grain Growth in a Zr Alloy.* **Bozzolo, N., et al.** : Materials Science Forum, 2007, Vols. 558-559, pp. 86-868.

7. **Cullity, B. D.** *Elements of X-ray Diffraction.* Reading : Addison-Wesley Publishing Company, Inc, 1978.

8. **Schwartz, Adam J, Kumar, Mukul and Adams, Brent L.** *Electron Backscatter Diffraction in Material Science.* New York : Kluwer Academic, 2000.

9. **George F. Vander Voort, William Van Geertruyden.** Specimen Preparation for Electron Backscatter Diffraction. Lake Bluff : Buehler Ltd.

10. **Mukherji, Anil K.** *Analytical Chemistry of Zirconium and Halfnium.* Oxford : Pergamon Press, 1970.

11. **Flanagan, Michelle E.** The Effect of Hydrogen on the Deformation Behavior of Zircaloy-4. *M.S. Thesis in Nuclear Engineering.* : Penn State University, December 2008.

12. **Philip A. Schweitzer, P. E.** *Corrosion Engineering Handbook.* New York : Marcel Dekker, Inc., 1996.

13. **Danielson, Paul E. and Albany, Teledyne Wah Chang.** Zirconium and Hafnium and Their Alloys. *Metallographic Techniques and Microstructures.* pp. 498-502.

14. **A. Yilmazbayhan, A. Motta, et al.** Structure of zirconium alloy oxides formed in pure water studied with synchrotron radiation and optical microscopy: relation to corrosion rate. *Journal of nuclear materials.* 2004. Vol. 324, pp. 6-22.

Appendix A

SEM polishing thick oxides

Sample preparations was done by using the diamond saw to section coupon and then mount in epoxy with 1.25 inch mold to use in Allied auto-polisher.

- Grinding (cool with running water)
    - 180 grit SiC paper
        - 100 rpm plate, 110 rpm head same direction
        - 4 Newton individual pressure
        - 1-2 min to flatten sample
    - 400 grit SiC paper
        - 100 rpm plate, 110 rpm head same direction
        - 4 Newton individual pressure
        - 2-4 min
    - 600 grit SiC paper
        - 120 rpm plate, 130 rpm head same direction
        - 9 Newton individual pressure
        - 4-6 min
    - 800 grit SiC paper
        - 120 rpm plate, 130 rpm head same direction
        - 9 Newton individual pressure
        - 6-8 min
    - 1200 grit SiC paper
        - 120 rpm plate, 130 rpm head same direction
        - 9 Newton individual pressure
        - 6-8 min
- Polishing
    - 1µm mono-crystalline Diamond suspension (Leco)
        - Imperial cloth
        - 110 rpm head, 130 rpm head same direction
        - 9 Newton individual pressure
        - 10 min (use green lube)
    - 0.05µm Colloidal Silica (Leco)
        - Imperial cloth
        - 110 rpm head, 130 rpm head same direction
        - 4 Newton individual pressure
        - 10 min (use DI water)

This procedure works well for samples with oxides thicker than 2µm or samples that have been nickel plated. Thinner oxides will flake off.

SEM polishing thin oxide

Sample preparations was done by using the diamond saw to section coupon and then mount in epoxy with 1.25 inch mold to use in Allied auto-polisher.

- Grinding (cool with running water)
    - 180 grit SiC paper
        - 100 rpm plate, 110 rpm head same direction
        - 4 Newton individual pressure
        - 1-2 min to flatten sample
    - 400 grit SiC paper
        - 100 rpm plate, 110 rpm head same direction
        - 4 Newton individual pressure
        - 2-4 min
    - 600 grit SiC paper
        - 120 rpm plate, 130 rpm head same direction
        - 9 Newton individual pressure
        - 6-8 min
    - 800 grit SiC paper
        - 120 rpm plate, 130 rpm head same direction
        - 9 Newton individual pressure
        - 6-8 min
- Polishing
    - 3µm polycrystalline Diamond suspension (Allied)
        - White label cloth
        - 110 rpm head, 130 rpm head same direction
        - 9 Newton individual pressure
        - 10 min (use green lube)
    - 1µm mono-crystalline Diamond suspension (Leco)
        - Imperial cloth
        - 110 rpm head, 130 rpm head same direction
        - 9 Newton individual pressure
        - 10 min (use green lube)
    - 0.05µm Colloidal Silica (Leco)
        - Imperial cloth
        - 110 rpm head, 130 rpm head same direction
        - 4 Newton individual pressure
        - 10 min

This procedure works very well for all oxide thicknesses. Very thin oxides remain intact.

Polarized light polishing

Sample preparations was done by using the diamond saw to section coupon and then mount in epoxy with 1.25 inch mold to use in Allied auto-polisher.

- Grinding (cool with running water)
    - 180 grit SiC paper
        - 100 rpm plate, 110 rpm head same direction
        - 4 Newton individual pressure
        - 1-2 min to flatten sample
    - 400 grit SiC paper
        - 100 rpm plate, 110 rpm head same direction
        - 4 Newton individual pressure
        - 2-4 min
    - 600 grit SiC paper
        - 120 rpm plate, 130 rpm head same direction
        - 9 Newton individual pressure
        - 6-8 min
    - 800 grit SiC paper
        - 120 rpm plate, 130 rpm head same direction
        - 9 Newton individual pressure
        - 6-8 min
- Polishing
    - 3µm polycrystalline Diamond suspension (Allied)
        - White label cloth
        - 110 rpm head, 130 rpm head same direction
        - 9 Newton individual pressure
        - 10 min (use green lube)
    - 1µm polycrystalline Diamond suspension (Allied)
        - Vel-cloth
        - 110 rpm head, 130 rpm head same direction
        - 9 Newton individual pressure
        - 20 min (use green lube)
    - 0.05µm Colloidal Silica (Leco) : Hydrogen peroxide (30%) 5:1 volume ratio
        - Chem-pol cloth
        - 110 rpm head, 130 rpm head counter direction
        - 4 Newton individual pressure
        - 30-60 min (Use with DI water)

OIM polishing

Sample preparations were as shown in Figure 3-2 and polished in an Allied auto-polisher.

- Grinding (cool with running water)
    - 180 grit SiC paper
        - 100 rpm plate, 110 rpm head same direction
        - 4 Newton individual pressure
        - 1-2 min to flatten sample
    - 400 grit SiC paper
        - 100 rpm plate, 110 rpm head same direction
        - 4 Newton individual pressure
        - 2-4 min
    - 600 grit SiC paper
        - 120 rpm plate, 130 rpm head same direction
        - 9 Newton individual pressure
        - 6-8 min
    - 800 grit SiC paper
        - 120 rpm plate, 130 rpm head same direction
        - 4 Newton individual pressure
        - 6-8 min
- Polishing
    - 3µm polycrystalline Diamond suspension (Allied)
        - White label cloth
        - 110 rpm head, 130 rpm head same direction
        - 4 Newton individual pressure
        - 10-15 min (use green lube)

The grains of the zirconium should be mildly observed under polarized light before moving on to colloidal silica.

    - 0.05µm Colloidal Silica (Leco) : Hydrogen peroxide (30%) 5:1 volume ratio
        - Chem-pol cloth
        - 110 rpm head, 130 rpm head counter direction
        - 4 Newton individual pressure
        - 20-30 min (Use with DI water)

The zirconium surface should not have any detectable flaws under microscope after mechanical polishing and should be maintained relatively flat. Over polishing with colloidal silica can depress the center of the sample due to the harder molybdenum on either side of the sample. The samples were then chemically swab etched.

VITA

Jacob L. Planinsek

Education:

The Pennsylvania State University, University Park, PA

Schreyer Honors College

B. S. Nuclear Engineering

Honors in Nuclear Engineering

Thesis Title: Electron and Optical Microscopy Analysis of Model Zirconium Alloys

Thesis Supervisor: Dr. Arthur Motta

Penn Foster Career School, Scranton, Pa

Tool and Die Certification

Experience:

Research Assistant
Dr. Arthur Motta research group, The Pennsylvania State University
Summer 2010

Research Assistant
Dr. Richard Bell research group, Penn State Altoona
Summer 2007-Spring 2010

Machinist
General Nuclear Corporation, New Stanton, PA
Tool and Die Apprenticeship
August 2002-January 2007

Machinist
S&K Machine Company, Latrobe, PA
February 2000-August 2002

Awards:

The University Trustee Scholarship

Exelon Nuclear Engineering Scholarship

Klevans Nuclear Engineering Scholarship

Society of Distinguished Alumni Trustee Scholarship

American Nuclear Society Decontamination, Decommissioning and Reutilization Scholarship

Activities:

American Nuclear Society

International Association for Hydrogen Energy

Alpha Nu Sigma Honors Society

Tau Beta Pi Engineering Honors Society

Phi Kappa Phi Honors Society

Golden Key International Honors Society